Research Square

Preprints are preliminary reports that have not undergone peer review.
They should not be considered conclusive, used to inform clinical practice,
or referenced by the media as validated information.

Homogeneity and strain localization promotes repeating seismic events on smooth faults during laboratory stick-slip experiments

Kiran Pandey

pandeykiran80@gmail.com

Terracon Consultants Inc

Navin Thapa

University of Memphis

Georg Dresen

Helmholtz Centre Potsdam - GFZ German Research Centre for Geosciences

Thomas HW Goebel

University of Memphis

Research Article

Keywords: Fault zone rheology, Acoustic emission, Repeating Earthquakes, Fault roughness, Strain localization

Posted Date: November 24th, 2026

DOI: https://doi.org/10.21203/rs.3.rs-9876644/v1

License: This work is licensed under a Creative Commons Attribution 4.0 International License.
Read Full License

Additional Declarations: No competing interests reported.

Homogeneity and strain localization promotes repeating seismic events on smooth faults during laboratory stick-slip experiments

Kiran Pandey[1,2*], Navin Thapa[1†], Georg Dresen[3†], Thomas HW Goebel[1†]

[1*]Center for Earthquake Research and Information , The University of Memphis, 3890 Central Ave, Memphis, 38152, Tennessee, USA.
[2]Geophysics, Terracon Consultants Inc, 11600 Lilburn Park Rd, St. Louis, 63146, Missouri, USA.
[3]German Research Centre for Geosciences GFZ, Helmholtz Centre Potsdam, Telegrafenberg, Potsdam, 14473, Brandenburg, Germany.

*Corresponding author(s). E-mail(s): pandeykiran80@gmail.com;
Contributing authors: nthapa@memphis.edu; georg.dresen@gfz.de;
thgoebel@memphis.edu;
†These authors contributed equally to this work.

Abstract

Repeating earthquakes are thought to be caused by slip on the same fault patch at varying times leading to highly coherent waveforms. Such events may be affected by heterogeneity, for instance, due to varying stress, fault roughness, and fault gouge composition. However, how roughness affects the generation of repeating events is poorly understood. Here, we detect repeating acoustic emissions (AEs) using time-domain cross-correlation between all possible event pairs and analyze their relationship with fault roughness in laboratory experiments conducted on cylindrical Westerly Granite samples. We observe a higher proportion of repeaters on polished saw-cut surfaces when AEs are localized within a narrow zone around the fault. A significant increase in the occurrence of repeaters is observed at higher differential stress, along with progressive spatial localization of AE events as the fault approaches failure. Repeating events are observed primarily in and around areas with high AE densities and are mostly localized along the principal slip surfaces. This highlights a close link between microseismicity and localized deformation prior to failure. High-resolution studies of small repeating events

before natural earthquakes may improve the understanding of fault properties and aseismic nucleation processes.

Keywords: Fault zone rheology, Acoustic emission, Repeating Earthquakes, Fault roughness, Strain localization

1 Introduction

Repeated failure of the same fault patch or asperity at different times produces highly coherent waveforms, and such seismic events are called repeaters [1–4]. In addition to waveform similarity, other criteria for classifying seismic events as repeaters include similar focal mechanisms, overlapping rupture areas, and magnitude [1, 5–7]. Repeating earthquakes occur as recurrent ruptures of a locked fault patch or asperities between locked and creeping portions of the fault [1, 6, 8]. In its simplest form, repeating events are analogous to stick-slip on laboratory faults where the "stick" phase represents frictionally locked asperity and the "slip" resembles asperity ruptures [6, 9–11].

Repeaters have been detected in a wide range of tectonic settings. Many repeaters are observed at transform plate boundaries where geodetic and other observations show low seismic coupling [12, 13], indicating that most of the slip is accommodated by fault creep [1, 6, 14–16]. Repeaters are also common along subduction zone interfaces with abundant microseismicity and varying interplate coupling, often exhibiting significant sporadic afterslip and spontaneous slow slip events [1, 17–19]. Similarly, repeaters (or highly coherent events) have been recorded at non tectonic regions like volcanoes [20–22] and landslides [23, 24]. These environments often promote strain localization, where deformation initially distributed across a broader region becomes increasingly focused within narrow zones along developing faults or slip surfaces as failure approaches [25, 26].

Earthquake repeaters provide insight into fault zone dynamics and are thought to be correlated with strain rate and fault creep [27]. Small repeating earthquakes along the San Andreas fault have been useful in estimating strain rate and moment release [1, 28, 29]. Furthermore, such earthquake repeaters are useful in measuring coseismic and postseismic velocity changes, which aids in understanding fault zone characteristics over time [30–32]. Uchida and Matsuzawa [33] demonstrated that repeaters are crucial for understanding slow-slip earthquakes and their relationship to fault creep in regions like the Tohoku-oki earthquake zone.

Numerous studies on natural fault systems have advanced our understanding of earthquake repeaters. However, the influence of various factors, such as differences in stress levels, fault roughness, and fault gouge composition, is not well studied. Here, we explore the role of fault surface heterogeneity in generating repeating acoustic emissions in controlled laboratory experiments.

2 Experiment, Data and Method

In the following, we discuss repeating seismic events observed during six different experiments on cylindrical Westerly granite samples (Tab. 1). The samples were 50 mm in diameter and 105 mm in length (Fig. 1; Supplementary Fig. S1). Experiments were conducted under varying boundary conditions. The samples contain a saw-cut fault or natural fracture, oriented at an angle of 30° to the loading axis. The fault surfaces were prepared using different techniques to achieve varying roughness. Polished planar surfaces (Smooth-1 and Smooth-2) were prepared by grinding with fine-grain (#290) silicon-carbide powder, while rough planar surfaces (Rough-1 and Rough-2) were prepared using coarser (#60) silicon-carbide powder.

Rough fractured surfaces (RoughFrac-1 and RoughFrac-2) were formed through direct fracturing to simulate natural roughness. The samples contained 1 mm wide notches at a 30° angle that guided the initial propagation of the fracture during axial loading at 75 MPa confinement. The samples were confined at 120 MPa and loaded axially until failure. The fresh fractures were locked by increasing the confining pressure to 150 MPa, followed by axial loading.

These different preparation techniques were used to prepare faults with varying initial roughness and heterogeneity, with visual characterization (CT scans) of similar fault structures [34]. Throughout these experiments, the samples were subjected to axial loading at a rate of 0.3 μ m/sec.

Table 1 Summary of experiments and resulting peak failure stresses and behaviors. Shown are experiment names with corresponding confining pressures, peak failure stresses, and failure behaviors.

Experiment	Confining Pressure (MPa)	Peak Failure Stress (MPa)	Failure Type
Smooth-1	120	440	Stick-slip
Smooth-2	120	480	Stick-slip
Rough-1	120	375	Stable sliding
Rough-2	120	410	Stable sliding
RoughFrac-1	150	345	Stick-slip
RoughFrac-2	150	365	Stick-slip

The AE activity in the sample during loading was measured by an array of sixteen 5 mm-diameter piezoceramic transducers with a resonant frequency of 2 MHz. Each transducer was connected to a high-speed digitizing board with a sampling frequency of 10 MHz and 16-bit amplitude resolution. The accuracy of AE location recordings is around 1 to 4 mm, and further information about AE hypocenter location is available in Stanchits et al. [35] and Goebel et al. [36]. The AEs in these experiments align roughly at 25° to 35° to the largest principal stress, σ_1 (Fig. 1).

Repeating event families were identified based on waveform similarity. All event waveforms were bandpass filtered between 0.01 and 2 MHz. Data filtering and processing were kept minimal to preserve the original characteristics of the waveforms. The

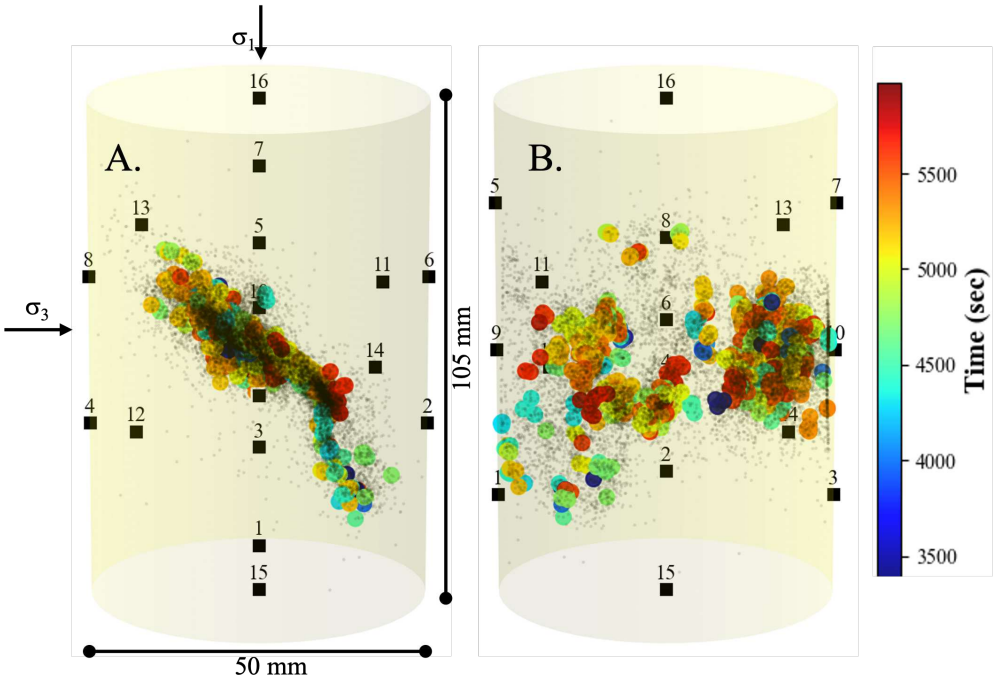


Fig. 1 Acoustic emission and repeating event locations in a fractured sample during stick slip. Acoustic emissions are colored as gray scatter, and repeating event origin times are highlighted by blue to red shades. Small filled square boxes represent AE sensor locations. (A) illustrates locations along fault direction ($\approx 30^\circ$ to principal stress direction along σ_1), while (B) depicts the AE distribution along the on-fault direction.

Akaike Information Criterion (AIC) [37, 38] was used to pick the arrival time of the direct P phase. We used 15 μs long waveforms from 5 μs before the P phase arrival to 10 μs after the P phase arrival. The similarity between two events was quantified by cross-correlating their waveforms at different lag times [1–3]:

$$C(\tau) = \frac{\sum_{t=1}^{N} f_x(t) f_y(t+\tau)}{\sqrt{\sum_{t=1}^{N} f_x(t)^2} \cdot \sqrt{\sum_{t=1}^{N} f_y(t+\tau)^2}} \tag{1}$$

where $C(\tau)$ is a normalized cross-correlation function between two waveforms f_x and f_y recorded at different times on the same channel, N is number of samples and τ is lag time. The signals were normalized by their root mean square amplitudes (Obspy Library; Krischer et al. [39]).

The waveforms were cross-correlated with a maximum allowable time shift of 5 μs. Each recorded event was cross-correlated with all other events in the catalog on the respective channel. Event pairs with a cross-correlation coefficient ≥ 0.95, observed on at least 7 channels, were grouped under the same repeating family (Fig. 2). Furthermore, if event pairs (A,B) and (B,C) are repeater pairs, then events A,B and C are grouped as a repeating family where A and C have cross-correlation coefficients ≥ 0.9.

No systematic dependence of the cross-correlation coefficient and the source receiver distance was observed (Supplementary Fig. S2).

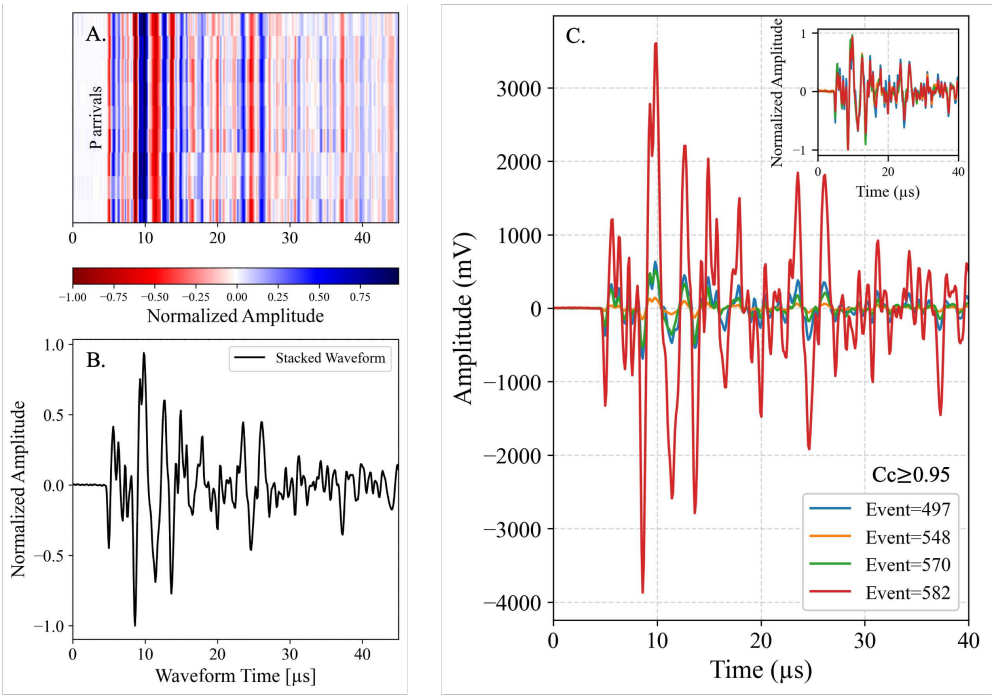


Fig. 2 Seismic event waveforms within a repeating family. Repeaters are detected based on highly coherent waveforms with cross-correlation coefficient ≥ 0.95. Panel A) shows amplitude normalized waveforms of AE within a repeating family as a color plot aligned along the P-phase arrival. Panel B) illustrates the stacked waveform of all the events within one repeating family. Panel C) shows representative waveforms for repeating members with cross-correlation coefficient ≥ 0.95 before amplitude normalization. The inset shows waveform similarity after amplitude normalization.

We employed a first-arrival polarity-based approach to identify the source types for each AE event. This procedure follows the polarity normalization approaches described by Kwiatek et al. [40] and implemented in AE studies [34]. We calculated an average first motion polarity across all transducers [34, 40, 41] to assign a source type to an AE event. The 3D array of transducers (Fig. 1) provides a good focal sphere coverage to record the AEs emitted during the experiments, which helps to determine the average source types. For each AE event, an average polarity, P_{ave}, was calculated as:

$$P_{\text{ave}} = \frac{1}{n} \sum_{i=1}^{n} \text{sign}(A_i) \tag{2}$$

where, n represents the number of transducers, and $\text{sign}(A_i)$ denotes polarity of events at each transducers [34, 41]. The events were then classified according to the value of P_{ave} into three categories [41]: compression-dominated events (C-type) for

$P_{\text{ave}} < -0.25$, shear-dominated events (S-type) for $-0.25 \leq P_{\text{ave}} \leq 0.25$, and tensile events (T-type) for $P_{\text{ave}} > 0.25$. These different source types of AE event likely represent distinct micromechanical processes [35, 41–43]. The shear events indicate frictional sliding along existing cracks or grain boundaries, whereas tensile events correspond to the opening or formation of micro-cracks under tensile stress. The compression events represent the compaction or closure of void spaces or weak asperities as stress increases.

Relative AE magnitudes were obtained by correcting the peak amplitude of waveforms recorded at each sensor A_i for geometric spreading with the source–receiver distance R_i and then taking the log of average distance corrected amplitude [34, 41, 44]:

$$M_{\text{AE}} = \log_{10} \sqrt{\frac{1}{n} \sum_{i=1}^{n} (A_i R_i)^2}. \tag{3}$$

We applied Principal Component Analysis (PCA) to study the spatial localization of AE events and repeaters. The PCA method reduces the number of dimensions in the data while maintaining as much variability as possible [45–47]. PCA identifies the axes of greatest spatial spread in the AE cloud. PC1 aligns with the direction of maximum variance. PC2 and PC3 capture the progressively smaller variances along the remaining orthogonal planes. By using PCA method, we categorize the spatial data into on-fault, along-fault, and fault-normal directions (Supplementary Fig. S3). This coordinate framework maps the localization of AEs and repeaters across varying fault conditions.

3 Results

We show results from six experiments conducted on polished and roughened saw-cut interfaces, and rough-fractured faults (Tab. 1). Here, we focus on the analysis of AEs during the first slip phase, which is controlled by the initial roughness of the fault. This allows us to understand the effects of the initial roughness of the fault in repeater generation and its role in influencing strain localization and AE behavior before fault smoothing becomes dominant in subsequent phases.

3.1 Repeater Abundance and Fault Heterogeneity

The occurrence of repeating events and their characteristics are strongly influenced by fault heterogeneity (Tab. 2). Polished planar faults, i.e., Smooth-1 and Smooth-2, show the highest proportion of repeaters, with 21% and 19%, respectively. These faults also support larger repeating family sizes, with Smooth-1 reaching up to 10 members and Smooth-2 reaching 13. Here, a repeating family size denotes the total number of AE events that repeat in that family. In contrast, rough faults, including RoughFrac-1, RoughFrac-2, Rough-1, and Rough-2, show significantly lower repeater proportions of 8%, 7%, 14%, and 10%, and maximum family sizes of 5, 6, 5, and 8, respectively. The rough planar faults, Rough-1 and Rough-2, exhibit slightly higher

Table 2 The proportion of repeating events and repeater failure types (shear, compression, and tensile) varies with fault surface condition and slip behavior. Rough-1 and Rough-2 exhibit stable sliding, whereas RoughFrac-1, RoughFrac-2, Smooth-1, and Smooth-2 exhibit stick-slip behavior. Maximum family size represents the number of events in the largest repeating family.

Experiment	All AE Count	Repeater %	Repeater Failure Type (%)			Max. Family Size
			Shear	Compression	Tensile	
Smooth-1	2113	21	48	49	3	10
Smooth-2	3326	19	67	30	3	13
Rough-1	3787	10	31	66	3	8
Rough-2	2072	14	8	91	1	5
RoughFrac-1	8476	8	14	84	12	5
RoughFrac-2	41350	7	10	89	1	6

repeater proportions and repeater family sizes, suggesting that asperity dynamics differ from those of RoughFrac.

The proportions of shear, tensile, and compression failure types in repeating events further highlight the differences between smooth and rough faults. Repeating events in polished planar faults, Smooth-1 and Smooth-2, are dominated by shear types (48% and 67%), followed by compression events (49% and 30%, respectively), with negligible tensile events (3% in both cases) (Tab. 2). In comparison, rough faults are dominated by compression-type repeaters, with RoughFrac-1 and RoughFrac-2 showing the repeater proportion at 84% and 89%, and Rough-1 at 91% and Rough-2 at 66%. Shear types are much less prominent on rough faults, accounting for 10%, likely because rough surfaces promote more compressive failure. These observations highlight the role of fault surface properties in controlling failure mechanisms.

Fault surface roughness limits the magnitude range and the total number of repeating acoustic emissions. All three types of experiments (polished planar, rough planar, and rough fracture) generate a peak repeater frequency at relative magnitudes between 2.0 and 2.5; however, there is a sharp difference in their upper-bound limits (Fig. 3). Polished planar faults (Smooth-1) produce a wide magnitude range from 1.7 to 4.8, whereas rough fractured faults (RoughFrac-1) limit the maximum magnitude to 3.5. Smooth surfaces promotes larger rupture areas supporting the generation of relatively larger magnitude repeaters.

3.2 Localization of Repeating Events in High-Stress Regions

Repeating acoustic emissions are predominantly observed during periods of high stress close to failure (Fig. 4). The occurrence of repeaters on polished planar faults (Smooth-1) begins when the differential stress reaches approximately 90% of the failure stress, which also coincides with a steady increase in AE rates (Supplementary Fig. S4). In contrast, rough faults show repeaters occurring from the early onset of loading (Fig. 4B & 4C), and the rate increases rapidly as the fault approaches failure. These observations highlight the role of surface roughness in affecting the timing of strain localization by allowing the asperities of rough faults to act as early rupture points.

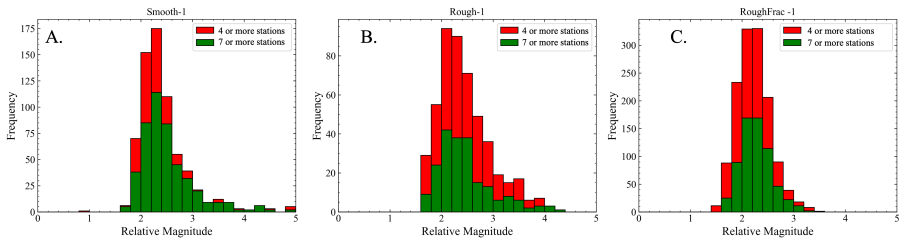


Fig. 3 Fault surface roughness controls the relative magnitude distribution of repeating acoustic emissions. The figure shows the distribution of relative sizes of repeating events observed in experiments under different fault conditions, using recordings from 4 or more stations (red) and 7 or more stations (green). (A) Smooth-1 corresponds to a polished planar fault experiment. (B) Rough-1 involves a rough planar fault experiment. (C) RoughFrac-1 describes a rough fracture fault experiment.

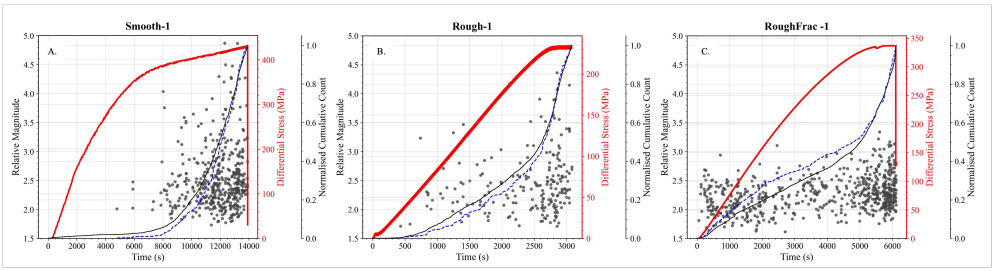


Fig. 4 The timing and evolution of repeating events are influenced by fault heterogeneity and surface roughness. The scatter points represent repeating events generated at various loading stages. The black solid curve represents the normalized cumulative number of AEs, and the blue dashed curve illustrates the normalized cumulative repeaters recorded during the experiments. The red curve represents differential stress (MPa). (A) Smooth-1: polished planar fault experiment; (B) Rough-1: rough planar fault experiment; (C) RoughFrac-1: rough fracture fault experiment.

Fault heterogeneity and state of stress control the spatial localization of AEs and repeating events. AE densities of rough faults show a few large patches of high AE density, whereas polished planar faults show smaller and more distributed clusters of high AE density reflecting larger contact area (Fig. 5). Repeating events on polished planar faults are spatially more distributed across the fault (Fig. 5A). Repeating events primarily cluster close to regions of high AE density. Repeaters on the rough planar surface and rough fracture are spatially more confined, clustering predominantly within the larger patches of high AE density and the distribution reflects the overall heterogeneity in AE locations (Fig. 5B & 5C).

The along-fault perspective shows the distribution of AEs and repeating events along the fault, focusing on variations across fault types (Fig. 6). In polished planar faults, such as Smooth-1, repeating events appear to be more evenly distributed, with clusters aligning closely along the fault slip direction. This distribution corresponds to a narrower zone with high AE density, as represented by the lighter regions in the

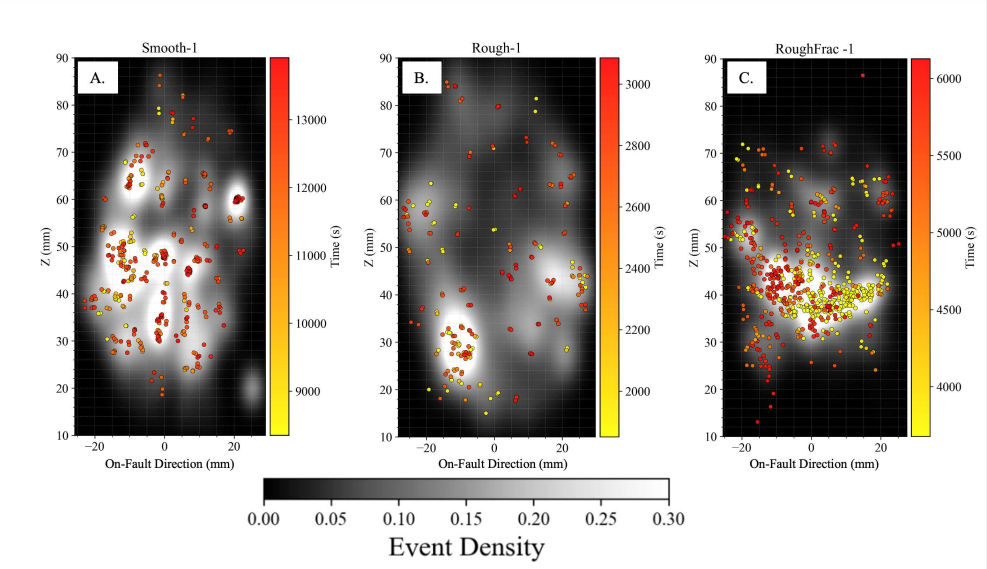


Fig. 5 Repeating events occur spatially localized around areas of higher AE density, possibly indicating areas of asperities. The gray-shaded background represents AE density, with shades of white indicating the highest event density in the on-fault direction. The colored scatter points, ranging from yellow to red, represent the repeating events over time in seconds. (A) Polished planar fault experiment (Smooth-1), (B) Rough planar fault experiment (Rough-1), and (C) Rough fracture fault experiment (RoughFrac-1).

background. On the other hand, repeaters in rough faults (Rough-1) are predominantly located near the center of the along-fault AE density zone, forming a notably tight and confined linear distribution (Fig. 6B). In RoughFrac-1, the repeater distribution is characterized by two spatially seperated clusters, one concentrated in the upper part ($\sim$ 55–75 mm) and another in the lower part ($\sim$ 40–50 mm) of the fault (Fig. 6C).

Fault surface roughness controls the spatial localization of repeating relative to the fault normal direction. Polished planar faults (Smooth-1 & Smooth-2) show a broader AE distribution and a localized repeater distribution, with Smooth-1 repeaters showing a sharp narrow peak within $\pm$ 1 mm, while Smooth-2 repeaters extend slightly broader to $\pm$ 2 to 3 mm from the principal slip zone. The rough planar faults (Rough-1 & Rough-2) show a repeater distribution within $\pm$ 3 to 4 mm from the slip surface, while AEs extend a little further. The rough fracture fault (RoughFrac-1 & RoughFrac-2) exhibits the broadest AE distribution, extending well beyond $\pm$ 7 mm, with most of the repeaters concentrated within $\pm$ 3 mm from the principal slip surface. The peak density of the repeaters is mostly higher and narrower than that of the AEs, possibly suggesting that most of the repeaters originate from localized asperities close to slip surfaces.

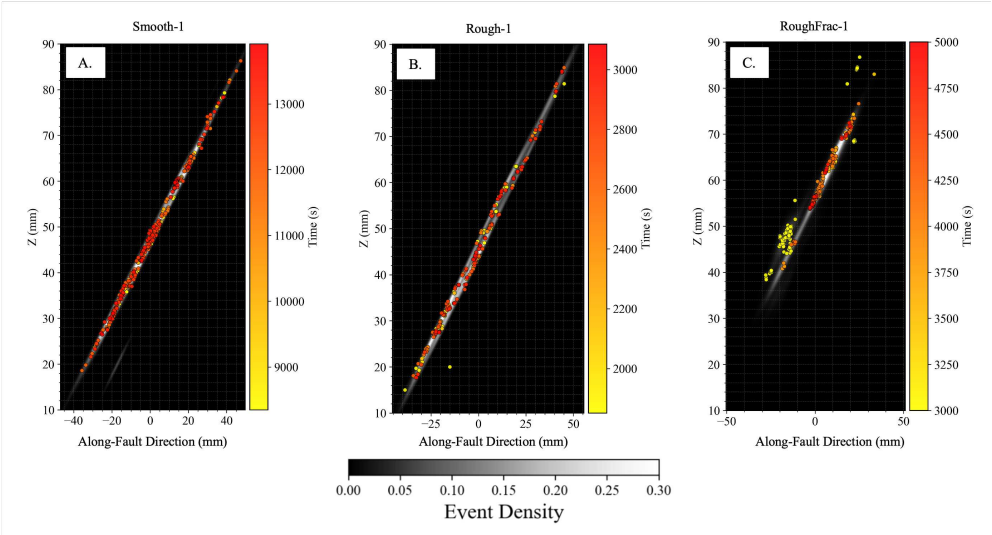


Fig. 6 The along-fault perspective shows that repeating events are spatially confined along a narrow slip zone, with the degree of confinement varying with fault surface roughness. The gray shaded background represents AE density, with shades of white indicating higher event density. The colored scatter points, ranging from yellow to red, represent the repeating events over time in seconds. (A) Polished planar fault experiment (Smooth-1), (B) Rough planar fault experiment (Rough-1), and (C) Rough fracture fault experiment (RoughFrac-1).

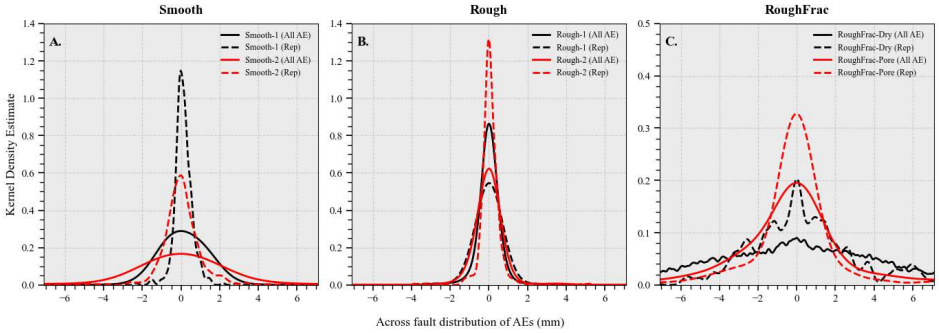


Fig. 7 Repeating events exhibit narrower spatial distributions in the fault normal direction compared to the entire AE catalogs. Panels A-C show kernel density estimates of the across-fault coordinate for each experiment type: Smooth (A), Rough (B), and RoughFrac (C). Within each panel, black curves correspond to Experiment-1 and red curves correspond to Experiment-2, with solid lines representing all AEs and dashed lines representing repeaters. All data were smoothed with an identical kernel density estimator using the same parameter settings.

3.3 Increase in shear-type events as failure approaches

As failure approaches, the fraction of shear-type events increases in most experiments, indicating favorable stress conditions and structural controls that promote shear over

tensile or compressive failure. This trend is observed in both AEs and repeaters for different fault conditions, highlighting the importance of shear events in fault dynamics near failure (Fig. 8).

In polished planar faults (Smooth-1), there is a steady increase in the fraction of shear-type AEs and repeaters with increasing differential stress, indicating gradual stress accumulation and strain concentration in localized fault areas. As the fault approaches failure, this accumulated strain energy is released mainly through shear dominant events (Fig. 8A & 8B). The dominance of shear repeaters is also observed in Table 1, where polished planar faults exhibit a higher proportion of shear failures compared to tensile and compressive modes. In the rough planar fault (Rough-1), C-type events dominate throughout for both AEs and repeaters; however, repeaters show a more pronounced transition toward shear-type dominance near failure compared to AEs, suggesting that repeating slip occurs preferentially along favorably oriented shear asperities as failure approaches (Fig. 8C & 8D). In contrast, the rough fracture experiment (RoughFrac-1) remains compression-type dominated throughout ($\sim$80 to 90%) for both AEs and repeaters, with S-type events exhibiting only a modest increase very close to failure, suggesting that the complex fracture network inhibits the development of organized shear failure (Fig. 8E & 8F).

4 Discussion

In this study, we observe that repeaters are usually found in and around the localized slip patches and high density damage zones (Fig. 5). As differential stress increases close to macroscopic Instability, these events tightly localize into a 2 to 4 mm band along the primary slip zone (Fig. 7). In many repeater studies, it is assumed that repeaters are the result of repeated rupture of isolated locked asperities surrounded by a creeping fault [2, 28]. Instead, our observations demonstrate that repeater occurrences are controlled by stress redistribution at the boundaries of localized slip zones. These repeating AEs likely relate to the repeating failure of grain-scale elements constituting asperities. We speculate that due to shear-enhanced compaction and localization, the probability of reactivating a similar 'nucleation spot' increases within these zones. Since the source area is much larger than a single grain, multiple grains breaking in the same spot appear as repeating events.

The occurrence and frequency of repeaters are governed primarily by fault surface heterogeneity, and the level of differential stress. In polished planar experiments, we observe a higher proportion of repeating events with larger repeating families and a wider magnitude range compared to rougher faults (Tab. 2). These smooth faults promote larger asperity contacts that distribute repeating sequences uniformly across the fault plane. Because larger asperities support higher levels of stress than smaller ones [48], these regions are capable of generating the relatively larger repeating sequences. In contrast, rough faults are characterized by irregular and isolated contact areas with heterogeneous stress fields, leading to more sporadic failure [49–51] and spatially confined repeater clusters at dominant asperities (Fig. 5). This leads to smaller percentage of repeaters relative to the total number of AEs and family sizes of repeating events. The narrower magnitude range and wider fault-normal distribution of repeaters in the

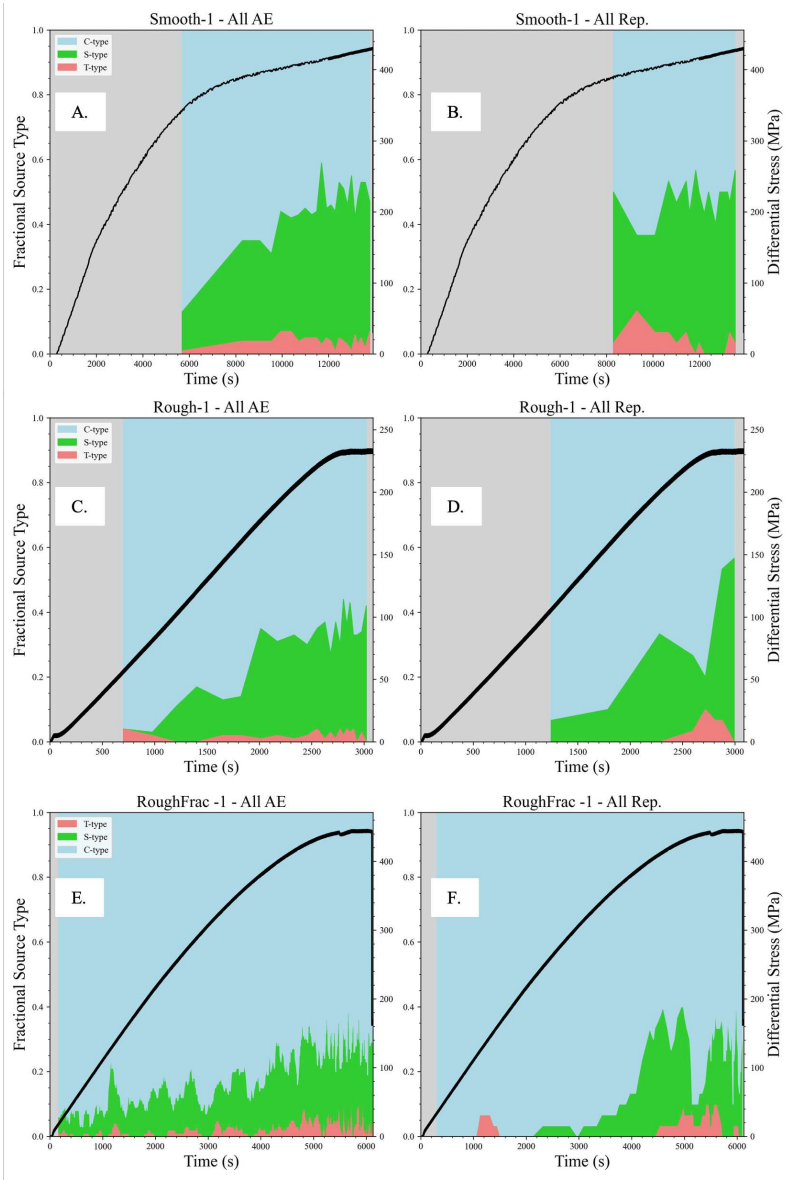


Fig. 8 The evolution of failure source types for AEs and repeating events in different experiments shows the increasing number of shear-type events as the fault approaches failure. The failure types include compression (C-type, blue), shear (S-type, green), and tensile (T-type, red) events. The black curve represents the increase in differential stress until the sample fails. The gray shaded region indicates the period before repeaters are detected. (A & B) show the source type evolution for all AEs and repeating events, respectively, in the polished planar fault experiment (Smooth-1). (C & D) show the source type evolution for the rough planar fault experiment (Rough-1). (E & F) illustrate the source type evolution for the rough fracture fault experiment (RoughFrac-1).

RoughFrac experiment suggests that complex fault surface structure limits the coalescence of larger scale ruptures, promoting smaller and spatially distributed failures [49]. The higher proportion of repeaters within localized strain zones confirms that they are driven by highly concentrated stress accumulation.

The generation of repeaters and their failure type show strong dependencies on stress level along the fault. At low differential stress, we observe a very low number of repeaters. As differential stress increases, the frequency of repeaters increases and most events for smooth and rough faults transition towards shear dominated mechanisms near failure (Fig. 8). This suggests a progressive localization of strain along the fault surface as failure approaches. We find that the surface roughness promotes earlier strain localization through asperity controlled failure. Repeaters in Rough and RoughFrac experiments occur from the early onset of loading, whereas in Smooth experiments, repeater activity begins only near ∼90% of the failure stress. Early repeaters at low differential stress are primarily influenced by compaction type events, particularly along rough faults, indicating localized compaction, pore collapse, and microfracturing within the fault gouge before organized shear failure. This change in millimeter-scale failure mechanism from compression to shear types serves as a precursor to fault slip, which is comparable to slip types mainly observed in natural earthquakes [34, 35, 40].

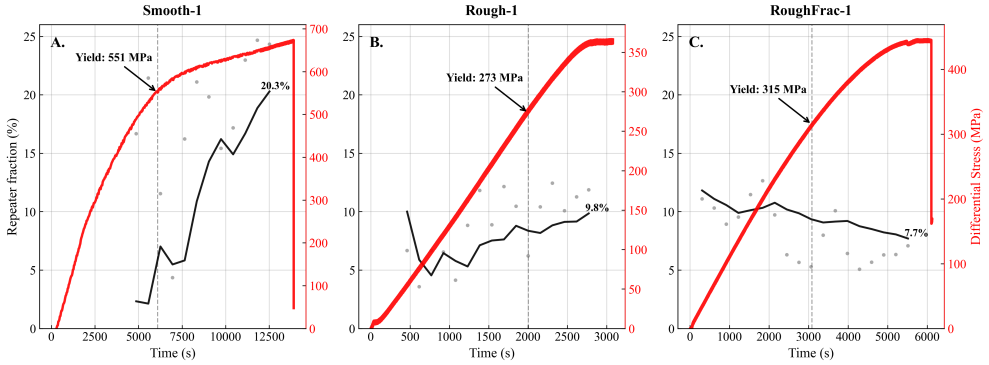


Fig. 9 Repeater fraction evolution reveals roughness-dependent localization. Red curves show differential stress (right axis) for Smooth-1 (A), Rough-1 (B), and RoughFrac-1 (C). Vertical dashed gray lines show yield points (where stress starts to deviate from linearity) estimated using the piecewise linear method. Gray dots show the repeater fraction computed in a sliding window of 10 % of the experiment run time with 50 % overlap, while solid black curves track the cumulative repeater fraction.

Repeater fraction, its temporal evolution, and its dependence on fault roughness together show that repeaters can measure the degree of fault slip localization. The cumulative repeater fraction reaches ≈ 21 % on Smooth-1, ≈ 10 % on Rough-1, and ≈ 8 % on RoughFrac-1 (Fig. 9). Spatial mapping of these repeaters shows highly localized planar zones on smooth surfaces but a wider, distributed pattern on rougher faults (Figs. 5 and 6). Smooth saw-cuts are known to have tighter fault plane orientations

and higher seismic coupling than rough faults [44], consistent with the more coherent planar slip zone we observe on smooth surfaces. The median event proximity also decreases as the fault approaches failure, suggesting a progressive localization of AE activity [52]. This also explains the late-stage increase in repeater fraction for the Smooth-1 and Rough-1 experiments after yield. Furthermore, we observe that the fraction of shear type repeaters increases as the fault approaches failure, suggesting that repeaters align with the focal mechanism of the dominant slip plane as localization occurs, indicating that fault roughness controls repeating earthquake generation.

The mechanism for repeaters varies with their source type, extending from slip for shear-type events to micro-mechanical adjustments for tensile and compaction AEs. Here, repeating shear-type events represent repeated slips on a specific fault patch. In contrast, the origin of nonshear type repeaters (compaction and tensile) in laboratory experiments requires consideration of evolving local stress and structural conditions. For compaction type AEs, which dominate the Rough faults, the process is likely due to the progressive compaction of grains, shear-enhanced compaction, and pore collapse in complex fracture networks [34, 35]. Because pure compaction represent irreversible structural damage, these sequences likely comprise tightly clustered repeaters [53] rupturing adjacent material within the damage zone. The localized sliding across contacting asperities and granular gouge is accommodated by combined grain fracturing, collapse of pore space, and shear across single or multiple grain boundaries.

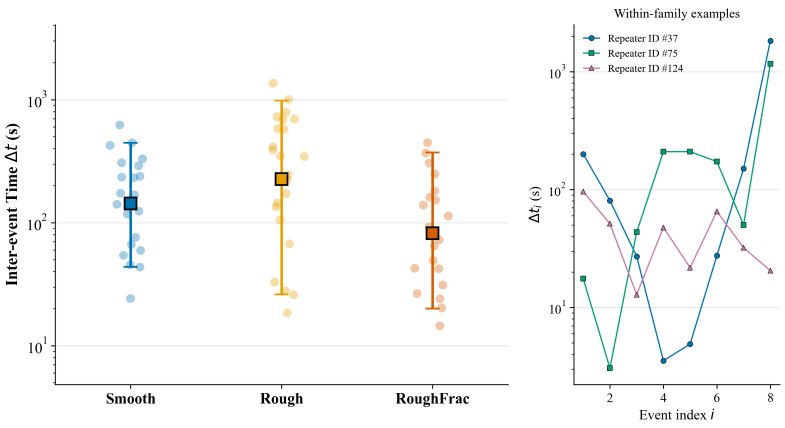


Fig. 10 Fault surface roughness shows no systematic control on repeater inter-event times. *(Left)* Circles represent the mean inter-event time (Δt, in s) for individual repeating families, filtered for statistical robustness ($n \geq 4$ events). Squares mark the group mean computed on a logarithmic scale, and the vertical bars span the 5th–95th percentile range of the family means within each group. *(Right)* Inter-event intervals Δt_i variability within repeater families showing erratic behavior within the family.

In natural fault systems, the recurrence intervals between repeating earthquakes systematically decrease as the fault approaches failure, reflecting progressive slip acceleration [19, 27]. However, in our laboratory experiments, we observe that the recurrence intervals between members of the same repeater family are erratic, with

inter-event times spanning a wide range regardless of fault roughness (Fig. 10). Similarly, unpredictable repeat intervals and burst type behavior are observed for some repeaters on complex natural faults [6, 54]. This highlights that while repeaters provide information about asperity failure and stress evolution, the recurrence times do not always show consistent patterns. This variance could be due to the sensitivity of laboratory asperities to minute local stress redistribution and the inherent variability of frictional properties [55].

Several studies suggest that repeaters occur along well-defined, single rupture planes [8, 50]. While repeaters from Smooth experiments are evenly distributed along a narrow slip zone, our observations from Rough experiments support more heterogeneous distribution. In these structurally complex cases, repeating events occur within a broader, off-fault damage zone. This suggests that the localized slip on a single frictional interface is not the only source of repeaters; rather, repeaters can also reflect the activation of multiple off-fault zones.

Fault surface maturity governs strain localization, rupture coalescence, and the occurrence of repeating earthquakes. Smooth (mature) faults, such as the creeping segments of the San Andreas, Hayward, and Calaveras faults localize strain into a narrow zone and produce a larger proportion of repeating earthquakes [1, 28]. In contrast, structurally rough, immature faults with heterogeneous contact stresses show less spatial localization and produce few repeaters. In these complex, early stage faults, complete spatial overlap of seismic sources is rare, and seismicity is dominated by spatially distributed repeaters [53] rather than strictly localized repeater [18, 30].

5 Conclusions

We examined the generation and behavior of repeating acoustic emission events across three distinct classes of faults: polished planar, rough planar, and rough fractured faults. We conclude that, in the laboratory setting, fault surface heterogeneity and the state of stress are the primary factors influencing the generation, spatial distribution, and source types of repeaters. These events were primarily localized in and around strong fault patches, where stress accumulates and releases over time. Furthermore, polished planar faults (Smooth) exhibited a higher percentage of repeaters with relatively larger magnitude repeating events. In contrast, rough faults were characterized by a relatively lower proportion of repeaters. The across fault distributions demonstrate that repeaters are more narrowly localized around the principal slip zone compared to the broader acoustic emission distribution. This indicates that repeating slip originates from localized asperities close to the slip surface, highlighting the role of surface roughness.

This study provides insights into the processes governing earthquake repeaters, asperity interactions, and fault stability. Understanding these dynamics offers key contributions to seismic hazard assessment where similar mechanisms may govern stress accumulation and release in natural seismic zones.

Author contributions. This study was a collaborative effort. All authors actively participated in material preparation. KP drafted the first version of the manuscript,

which was then revised by the entire team. All authors approved the final submitted version.

Supplementary information. Supplementary information accompanies this paper and provides additional figures that support the interpretations presented in the main text. Specifically, this document includes: detailed schematics and images of the experimental setup and fault geometry (Figure S1); plots demonstrating that cross-correlation has no systematic dependency on source-receiver distance (Figure S2); a visual definition of the principal component axes used for AE locations (Figure S3); and differential stress versus time curves highlighting the timing of repeater development across different fault roughnesses (Figure S4).

Acknowledgments. This research and K.P. were supported by NSF grant 2336144. T.G. was supported by the U.S. Department of Energy (DE-SC0022534). The authors also thank the German Research Center for Geosciences for providing the opportunity and facilities for conducting experiments. The authors express their gratitude for the constructive conversations at conferences.

References

[1] Uchida, N., Bürgmann, R.: Repeating earthquakes. Annual Review of Earth and Planetary Sciences **47**(1), 305–332 (2019)

[2] Schaff, D.P., Beroza, G.C.: Improvements in the location of repeating earthquakes using cross-correlation and double-difference methods: A case study of parkfield, california. Bulletin of the Seismological Society of America **104**, 1841–1856 (2014) https://doi.org/10.1785/0120130260

[3] Ellsworth, W.: Characteristic earthquakes and long-term earthquake forecasts: Implications of central california seismicity. In: Urban Disaster Mitigation: The Role of Engineering and Technology, pp. 1–14. Elsevier, ??? (1995)

[4] Chamberlain, C.J., Hopp, C.J., Boese, C.M., Warren-Smith, E., Chambers, D., Chu, S.X., Michailos, K., Townend, J.: Eqcorrscan: Repeating and near-repeating earthquake detection and analysis in python. Seismological Research Letters **89**(1), 173–181 (2018)

[5] Gao, D., Kao, H., Wang, B.: Misconception of waveform similarity in the identification of repeating earthquakes. Geophysical Research Letters **48**(13), 2021–092815 (2021)

[6] Waldhauser, F., Schaff, D.P.: A comprehensive search for repeating earthquakes in northern california: Implications for fault creep, slip rates, slip partitioning, and transient stress. Journal of Geophysical Research: Solid Earth **126**(11), 2021–022495 (2021)

[7] Cesca, S., Niemz, P., Dahm, T., Ide, S.: Anti-repeating earthquakes and how to explain them. Communications Earth & Environment **5**(1), 158 (2024)

[8] Sammis, C.G., Rice, J.R.: Repeating earthquakes as low-stress-drop events at a border between locked and creeping fault patches. Bulletin of the Seismological Society of America **91**(3), 532–537 (2001)

[9] Brace, W.: Laboratory studies of stick-slip and their application to earthquakes. Tectonophysics **14**(3-4), 189–200 (1972)

[10] Dieterich, J.H.: Time-dependent friction and the mechanics of stick-slip. Pure and applied geophysics **116**, 790–806 (1978)

[11] Byerlee, J.: The mechanics of stick-slip. Tectonophysics **9**(5), 475–486 (1970)

[12] Bird, P., Kagan, Y.Y., Jackson, D.D.: Plate tectonics and earthquake potential of spreading ridges and oceanic transform faults. In: Stein, S., Freymueller, J.T. (eds.) Plate Boundary Zones, pp. 203–218. American Geophysical Union, Washington, DC (2002)

[13] Peng, W., Radiguet, M., Pathier, E., Chen, K.H.: Fault coupling on a creeping thrust fault: Joint inversion using geodetic data and repeating earthquakes. Journal of Geophysical Research: Solid Earth **128**(9), 2023–026843 (2023)

[14] Bürgmann, R., Schmidt, D., Nadeau, R., d'Alessio, M., Fielding, E., Manaker, D., McEvilly, T., Murray, M.: Earthquake potential along the northern hayward fault, california. Science **289**(5482), 1178–1182 (2000)

[15] Chaussard, E., Bürgmann, R., Fattahi, H., Johnson, C., Nadeau, R., Taira, T., Johanson, I.: Interseismic coupling and refined earthquake potential on the hayward-calaveras fault zone. Journal of Geophysical Research: Solid Earth **120**(12), 8570–8590 (2015)

[16] Bohnhoff, M., Wollin, C., Domigall, D., Küperkoch, L., Martínez-Garzón, P., Kwiatek, G., Dresen, G., Malin, P.E.: Repeating marmara sea earthquakes: indication for fault creep. Geophysical Journal International **210**(1), 332–339 (2017)

[17] Gardonio, B., Marsan, D., Lengliné, O., Enescu, B., Bouchon, M., Got, J.-L.: Changes in seismicity and stress loading on subduction faults in the kanto region, japan, 2011–2014. Journal of Geophysical Research: Solid Earth **120**(4), 2616–2626 (2015)

[18] Igarashi, T.: Spatial changes of inter-plate coupling inferred from sequences of small repeating earthquakes in japan. Geophysical Research Letters **37**(20) (2010)

[19] Uchida, N., Matsuzawa, T., Hasegawa, A., Igarashi, T.: Interplate quasi-static slip off sanriku, ne japan, estimated from repeating earthquakes. Geophysical Research Letters **30**(15) (2003)

[20] Ratdomopurbo, A., Poupinet, G.: Monitoring a temporal change of seismic velocity in a volcano: application to the 1992 eruption of mt. merapi (indonesia). Geophysical Research Letters **22**, 775–778 (1995)

[21] Hotovec-Ellis, A.J., Vidale, J.E., Gomberg, J., Thelen, W., Moran, S.C.: Changes in seismic velocity during the first 14 months of the 2004–2008 eruption of mount st. helens, washington. Journal of Geophysical Research: Solid Earth **120**, 6226–6240 (2015)

[22] Petersen, T.: Swarms of repeating long-period earthquakes at shishaldin volcano, alaska, 2001–2004. Journal of Volcanology and Geothermal Research **166**, 177–192 (2007)

[23] Poli, P.: Creep and slip: seismic precursors to the nuugaatsiaq landslide (greenland). Geophysical Research Letters **44**, 8832–8836 (2017)

[24] Yamada, M., Mori, J., Matsushi, Y.: Possible stick-slip behavior before the rausu landslide inferred from repeating seismic events. Geophysical Research Letters **43**, 9038–9044 (2016)

[25] Wong, T.-f., Baud, P.: The brittle-ductile transition in porous rock: A review. Journal of Structural Geology **44**, 25–53 (2012)

[26] Kaunda, R.B.: Role of localized elevated pore pressures and strain localization mechanisms in slope stability problems. In: Modeling in Geotechnical Engineering, pp. 183–203. Elsevier, ??? (2021)

[27] Nadeau, R.M., Foxall, W., McEvilly, T.: Clustering and periodic recurrence of microearthquakes on the san andreas fault at parkfield, california. Science **267**(5197), 503–507 (1995)

[28] Nadeau, R.M., McEvilly, T.V.: Seismological studies at parkfield v: Characteristic microearthquake sequences as fault-zone drilling targets. Bulletin of the Seismological Society of America **88**, 790–795 (1998)

[29] Becker, D., Martínez-Garzón, P., Wollin, C., Kılıç, T., Bohnhoff, M.: Variation of fault creep along the overdue istanbul-marmara seismic gap in nw türkiye. Geophysical Research Letters **50**(6), 2022–101471 (2023)

[30] Schaff, D.P., Beroza, G.C.: Coseismic and postseismic velocity changes measured by repeating earthquakes. Journal of Geophysical Research: Solid Earth **109**(B10) (2004)

[31] Li, L.: Depth-dependence of post-seismic velocity changes in and near source area of the 2013 m7. 0 lushan earthquake revealed by s coda of repeating events. Tectonophysics **717**, 302–310 (2017)

[32] Peng, Z., Ben-Zion, Y.: Temporal changes of shallow seismic velocity around the karadere-düzce branch of the north anatolian fault and strong ground motion. Pure and Applied Geophysics **163**, 567–600 (2006)

[33] Uchida, N., Matsuzawa, T.: Pre-and postseismic slow slip surrounding the 2011 tohoku-oki earthquake rupture. Earth and Planetary Science Letters **374**, 81–91 (2013)

[34] Goebel, T.H., Schuster, V., Kwiatek, G., Pandey, K., Dresen, G.: A laboratory perspective on accelerating preparatory processes before earthquakes and implications for foreshock detectability. Nature Communications **15**(1), 5588 (2024)

[35] Stanchits, S., Vinciguerra, S., Dresen, G.: Ultrasonic velocities, acoustic emission characteristics and crack damage of basalt and granite. Pure and Applied Geophysics **163**, 975–994 (2006)

[36] Goebel, T., Becker, T., Schorlemmer, D., Stanchits, S., Sammis, C., Rybacki, E., Dresen, G.: Identifying fault heterogeneity through mapping spatial anomalies in acoustic emission statistics. Journal of Geophysical Research: Solid Earth **117**(B3) (2012)

[37] Akaike, H.: A new look at the statistical model identification. IEEE transactions on automatic control **19**(6), 716–723 (1974)

[38] Kurz, J.H., Grosse, C.U., Reinhardt, H.-W.: Strategies for reliable automatic onset time picking of acoustic emissions and of ultrasound signals in concrete. Ultrasonics **43**(7), 538–546 (2005)

[39] Krischer, L., Megies, T., Barsch, R., Beyreuther, M., Kroeger, T.M., Li, C., Lass, S.: Obspy: a bridge for seismology into the scientific python ecosystem. Computational Science & Discovery **8**(1), 014003 (2015) https://doi.org/10.1088/1749-4699/8/1/014003

[40] Kwiatek, G., Goebel, T., Dresen, G.: Seismic moment tensor and b value variations over successive seismic cycles in laboratory stick-slip experiments. Geophysical Research Letters **41**(16), 5838–5846 (2014)

[41] Zang, A., Christian Wagner, F., Stanchits, S., Dresen, G., Andresen, R., Haidekker, M.A.: Source analysis of acoustic emissions in aue granite cores under symmetric and asymmetric compressive loads. Geophysical Journal International **135**(3), 1113–1130 (1998)

[42] Lei, X.: How do asperities fracture? an experimental study of unbroken asperities. Earth and Planetary Science Letters **213**(3-4), 347–359 (2003)

[43] Lei, X., Nishizawa, O., Kusunose, K., Satoh, T.: Fractal structure of the hypacenter distributions and focal mechanism solutions of acoustic emission in two granites of different grain sizes. Journal of Physics of the Earth **40**(6), 617–634 (1992)

[44] Dresen, G., Kwiatek, G., Goebel, T., Ben-Zion, Y.: Seismic and aseismic preparatory processes before large stick–slip failure. Pure and Applied Geophysics **177**, 5741–5760 (2020)

[45] Jolliffe, I.T., Cadima, J.: Principal component analysis: a review and recent developments. Philosophical transactions of the royal society A: Mathematical, Physical and Engineering Sciences **374**(2065), 20150202 (2016)

[46] Pearson, K.: Liii. on lines and planes of closest fit to systems of points in space. The London, Edinburgh, and Dublin philosophical magazine and journal of science **2**(11), 559–572 (1901)

[47] Hotelling, H.: Analysis of a complex of statistical variables into principal components. Journal of educational psychology **24**(6), 417 (1933)

[48] Selvadurai, P., Glaser, S.: Asperity generation and its relationship to seismicity on a planar fault: A laboratory simulation. Geophysical Journal International **208**(2), 1009–1025 (2017)

[49] Goebel, T.H., Kwiatek, G., Becker, T.W., Brodsky, E.E., Dresen, G.: What allows seismic events to grow big?: Insights from b-value and fault roughness analysis in laboratory stick-slip experiments. Geology **45**(9), 815–818 (2017)

[50] Cochran, E.S., Page, M.T., Elst, N.J., Ross, Z.E., Trugman, D.T.: Fault roughness at seismogenic depths and links to earthquake behavior. The Seismic Record **3**(1), 37–47 (2023)

[51] Thapa, N., Dresen, G., Goebel, T.H.: Does b-value increase with pore-pressure?: Insights from laboratory experiments and induced seismicity. Geophysical Research Letters **52**(11), 2025–115740 (2025)

[52] Kwiatek, G., Martínez-Garzón, P., Goebel, T., Bohnhoff, M., Ben-Zion, Y., Dresen, G.: Intermittent criticality multi-scale processes leading to large slip events on rough laboratory faults. Journal of Geophysical Research: Solid Earth **129**(3), 2023–028411 (2024)

[53] Zhou, Y., Ghosh, A.: Abundant quasi-repeating earthquakes occurring within repeater sequences on the erkenek-pütürge fault (se turkey). Geophysical Research Letters **52**(6), 2024–114367 (2025)

[54] Chen, K.H., Bürgmann, R., Nadeau, R.M.: Do earthquakes talk to each other?

triggering and interaction of repeating sequences at parkfield. Journal of Geophysical Research: Solid Earth **118**(1), 165–182 (2013)

[55] Beeler, N.M., Tullis, T., Junger, J., Kilgore, B., Goldsby, D.: Laboratory constraints on models of earthquake recurrence. Journal of Geophysical Research: Solid Earth **119**(12), 8770–8791 (2014)

Supplementary Files

This is a list of supplementary files associated with this preprint. Click to download.

- SupplementalPandeyetalHomogeneityandstrainlocalizationpromotesrepeatingseismicevents.zip